SUMMARY

The liquid-vapor data up to 200 atm. given here along with the liquid-vapor data up to 136 atm. of Sinor et al. and the solid-vapor data up to 140 atm. of Hiza and Kidnay provide a fairly complete set of consistent phase equilibria data for the helium-methane system. The major discrepancy between the sets of data occurred in the gas phase and in a temperature region where a simple test with enhancement factors shows that the present data follow a more reasonable course than those of Sinor et al. The isobaric consistency test applied indicates the probability that one isotherm in each set of liquid phase data is suspect in at least a portion of the pressure range, but in general the discrepancies are not very large. These new data provide adequate evidence that the old data of Kharakhorin and, to a lesser extent, those of Gonikberg and Fastovskii, are incorrect. Measurements of the three-phase locus and possibly some confirming measurements in the regions just below and above the triple-point temperature of methane and near the critical temperature of methane would be a valuable addition to the data for the helium-methane system.

NOTATION

ΔH_s = pseudo heat of solution, as defined by Equation (1)
K = ratio of mole fraction in gas phase to that in the liquid phase
p_0 = vapor pressure, atm.
T = temperature, °K.
x = mole fraction in liquid phase
y = mole fraction in gas phase
π = total pressure, atm.

Subscripts

1 = methane
2 = helium
0 = pure component

LITERATURE CITED

1. Hiza, M. J., and A. J. Kidnay, "Advances in Cryogenic Engineering," K. D. Timmerhaus, ed., Vol. 11, p. 338, Plenum Press, New York (1966).
2. Kharakhorin, F. F., *Inz. Fiz. Zhur.*, 2, No. 5, 55-59 (1959). Translation available at Special Library Assoc., Translations Center, Chicago.
3. Herring, R. N., and P. L. Barrick, "International Advances in Cryogenic Engineering," K. D. Timmerhaus, ed., Vol. 10, p. 151, Plenum Press, New York (1965).
4. Kirk, B. S., and W. T. Ziegler, *ibid.*, p. 160.
5. Sinor, J. E., D. L. Schindler, and Fred Kurata, *A.I.Ch.E. J.*, 12, No. 2, 353-357 (1966).
6. Gonikberg, M. G., and W. G. Fastovskii, *Acta Physicochim. URSS*, 13, 399-404 (1940).
7. Glasstone, Samuel, "Thermodynamics for Chemists," p. 324, Van Nostrand, New York (1947).

Manuscript received July 13, 1966; revision received October 17, 1966; paper accepted October 17, 1966.

Three Turbulent Drag Coefficients in Beds of Spheres

JOHN A. TALLMADGE

Drexel Institute of Technology, Philadelphia, Pennsylvania

Form, shear, and total drag have been studied in the 2,500 to 65,000 range of Reynolds number over a wide range of porosity by using the data of Thodos and co-workers. The effect of Reynolds number was found to be the —0.14 power for form drag, the —0.19 power for total drag, and the —0.5 and higher power for shear drag, so that the ratio of shear drag to total drag decreased from about 16% to less than 5% with increasing Reynolds numbers. For the 2,500 to 6,000 range of Reynolds number, experimental evidence supports the apparently analogous behavior between average shear drag and average heat flux. Limitations and related evidence of this behavior are also discussed. Methods are suggested for estimating drag ratios and coefficients by using the correlation of this work.

Where the same characteristic area and velocity are used to define drag coefficients, the total drag may be considered as equal to the sum of the shear drag and the pressure (or form) drag as follows:

$$f_t = f_s + f_p \qquad (1)$$

Knowledge of the interrelationships of these types of drag over a range of velocities contributes to the understanding of several phenomena, including the relative contributions of shear and form drag, the relationship between transport rates and pressure drop, and the differences among the mechanisms. Such understanding would be helpful in the determination of optimum flow rates.

Consider the case of turbulent flow in particulate beds. Although the total drag is relatively easy to determine from pressure drop measurements, shear drag and form drag are more difficult to measure. No direct measurements of shear drag have been reported and only recently have any precise measurements of form drag in beds of solids become available (*16*). The form drag work of Wentz and Thodos (*16*) has special importance because total drag was also measured on the same beds at the same conditions.

It might seem that the dependence of shear drag on velocity could easily be determined from Equation (1) and the existing correlations for form drag and total drag

TABLE 1. TYPICAL DATA

Run No.	31	45	77	89
Data of Wentz (*11*)				
Run No.	8	5	2	6
ϵ	0.354	0.480	0.743	0.882
$N_{Re}(1-\epsilon)$	1,650	3,880	5,690	7,661
f_t/ϵ^2	9.35	2.92	0.685	0.320
f_p/ϵ^2	7.92	2.38	0.587	0.297
Calculated f_s/ϵ^2	1.43	0.54	0.098	0.023
N_{Re}*	2,550	7,460	22,140	64,920
Drag numbers*				
$f_t/2$	0.586	0.336	0.189	0.124
$f_p/2$	0.496	0.274	0.162	0.115
$f_s/2$	0.090	0.062	0.027	0.009
Porosity adjusted drag*				
$f_t\,\epsilon/2$	0.208	0.162	0.140	0.110
$f_p\,\epsilon/2$	0.176	0.132	0.120	0.102
$f_s\,\epsilon/2$	0.032	0.030	0.020	0.008
Bed	Packed	Packed	Distended	Distended
Cubic center	Body	None	Face	None

* Values from Tables 2 to 4, after rounding.

(*16*). However, those correlations were developed with a restriction; it was implicity assumed that the functional dependence of form drag on N_{Re} was identical to that of total drag on N_{Re}. This assumption is a good approximation for correlating form drag at the flow rates studied. However, this assumption is not valid for determining the effect on N_{Re} on shear drag by use of Equation (1), because it erroneously implies that the mechanisms giving rise to shear and form drag are similar.

Therefore, to determine the influence of velocity on shear drag, it is necessary to develop new correlations for f_p and f_t from the Wentz and Thodos results. It will be assumed throughout this paper that the influence of Reynolds number on each of the three drag modes (shear, form, and total) may be different.

PURPOSE

The first objective of this paper is the determination of the functional dependence of shear, form, and total drag on Reynolds number (for turbulent flow through beds of packed and distended spheres over the range of porosity and Reynolds number for which the form drag data are available). This was done by developing suitable correlations for form and total drag and examining the values of shear drag obtained by using Equation (1). Two other objectives involve the discussion of the apparently analogous behavior between average shear drag and average heat flux and the comparison of methods for estimating drag ratios and drag coefficients.

DRAG DEFINITIONS

We chose by definition the following dimensionless forms of velocity (N_{Re}) and force, based on a velocity in the bed (u_b) and the surface area of the particles (A_s):

$$N_{Re} = \left(\frac{D\epsilon}{1-\epsilon}\right)\frac{U_b\rho}{\mu} = \frac{DU_s\rho}{\mu(1-\epsilon)} = \frac{DG}{\mu(1-\epsilon)} \quad (2)$$

$$\frac{f_s}{2} = \frac{F_s}{\rho U_b^2 A_s} = \frac{\tau_s\epsilon^2}{\rho U_s^2} = \frac{\tau_s\rho\epsilon^2}{G^2} \quad (3)$$

$$\frac{f_t}{2} = \frac{F_t}{\rho U_b^2 A_s} = \frac{\Delta P\epsilon^2 A_x}{\rho U_s^2 A_s} = \frac{\Delta P\rho D\epsilon^2}{6G^2L(1-\epsilon)} \quad (4)$$

$$\frac{f_p}{2} = \frac{F_n}{\rho U_b^2 A_s} = \frac{I_n\epsilon^2}{2\pi\rho U_s^2} = \frac{I_n\rho\epsilon^2}{2\pi G^2} \quad (5)$$

The integral of normal stress ($I_n = 2\pi F_n/A_s$), which appears in the form drag expression, is (*16*)

$$I_n = \int_o^{\pi/2} \sin^2\alpha\, d\alpha \int_o^{2\pi} (P_n - P_s)\cos\beta\, d\beta \quad (5a)$$

Other aspects of these definitions are discussed in Appendix *C*.†

The values of dimensionless velocity and force given previously (*16*) were apparently based on a velocity external to the bed. Their superficial Reynolds numbers and drag coefficients were adjusted to be consistent with the definitions given above and with the Reynolds numbers used in other correlations (*10, 15*). All fifty-one form drag runs reported by Wentz (*14*) were converted accordingly. Typical values are shown in Table 1. A complete tabulation of the data in the notation of this paper is given in Table 2 (packed beds), Table 3 (distended beds), and Table 4 (porosity adjusted drag coefficients), which are given elsewhere.†

RANGE OF N_{Re} AND OTHER CONDITIONS

The conditions of primary interest here are those reported in the form drag article by Wentz and Thodos (*16*). Those workers studied a wide range of porosity (0.35 to 0.88) and a moderate range of Reynolds number (2,600 to 65,000).

The spheres in those runs were fixed in various cubic orientations by 0.018 in. diameter wires, both in packed and in distended beds. It is believed that what those authors called packed beds were actually slightly distended beds due to the wires. Because no wire correction on drag was made, their reported values of form and total drag are somewhat distorted by unknown but probably small amounts.

The ratio of bed diameter to particle diameter was constant at about 11 (1.23 in. O.D. spheres and a 14 in. I.D.

† Deposited as document 9351 with the American Documentation Institute, Photoduplication Service, Library of Congress, Washington 25, D. C., and may be obtained for $1.25 for photoprints or 35-mm. microfilm.

tube). The wall effect of channeling was minimized by cutting off part of the peripheral spheres to obtain a close fit to the cylindrical tube. The ratio of bed length to particle diameter varied from 3 to 8 (five layers of spheres), but end effects were minimized in all form drag tests and were corrected for in the total drag tests by doing tests on the spheres in the central layer. Each of two packed beds (ϵ = 0.354 and 0.480) and four distended beds (ϵ = 0.615 to 0.882) were tested over a four- or fivefold range of velocity, usually with eight runs per bed.

DRAG CORRELATIONS (LITERATURE)

Most of the pressure drop data for packed beds have been taken at lower values of Reynolds number than the 2,500 to 65,000 range of interest here or with smaller ranges of porosity. Ergun's data (*2*) were taken at N_{Re} below 400, and his correlation is based on data below Reynolds numbers of 3,000. Martin et al. (*8*) studied pressure drop through stacked spheres at Reynolds numbers from 2 to 20,000 but porosities were 0.26 to 0.48; they did not find an equation which correlated all their data.

In their first paper (*15*), Wentz and Thodos reported total drag results for the same beds (plus one more) over the same range of Reynolds numbers and porosity used for the form drag studies. They also used, with some exceptions, the identical flow rates and thus identical Reynolds numbers. As a result, most of the total drag data reported for the same conditions (*14*) are taken directly from pressure drop data. However, some have probably been interpolated from their correlation (*12*), which is in equivalent form

$$\frac{f_t\,\epsilon}{2} = \frac{0.0585}{N_{Re}^{0.05} - 1.20} \qquad (6a)$$

Equation (*6a*) has been adjusted by a factor of 6 (to be consistent with the total drag definition used here) and has been divided by 1.13 to correct for end effects, in accordance with the same change made by Wentz and Thodos (*16*). The authors indicated that the three-constant form of Equation (*6a*) was selected to describe a slight deviation from log-log linearity at smaller Reynolds number.

In their second paper (*16*), Wentz and Thodos reported determination of form drag by integration of the normal pressure. Their pressures were measured at the test sphere surface as a function of two angular coordinates so that 111 pressure measurements were made per run. From these measurements, values equivalent to (f_p/ϵ^2) were calculated by evaluation of the net normal stress integral described by Equation (*5a*). Wentz and Thodos then correlated their form drag and total drag values using the same functional dependence on Reynolds number. In the notation of this paper, their correlations are

$$\frac{f_t}{2}\,\epsilon^{4/3} = 0.486\,[N_{Re}(1-\epsilon)]^{-1/6} \qquad (6b)$$

$$\frac{f_p}{2}\,\epsilon^{4/3} = 0.428\,[N_{Re}(1-\epsilon)]^{-1/6} \qquad (7)$$

FORM AND TOTAL DRAG

Equations (*6b*) and (*7*) are not suitable for the purposes of this paper because the exponents on N_{Re} were assumed to be identical.

We first developed a new correlation of form drag and Reynolds number as described in Appendix *A*. In brief, drag data of Wentz (*14*) were fit, for each of six beds, to a linear log-log relationship and cross fit at three

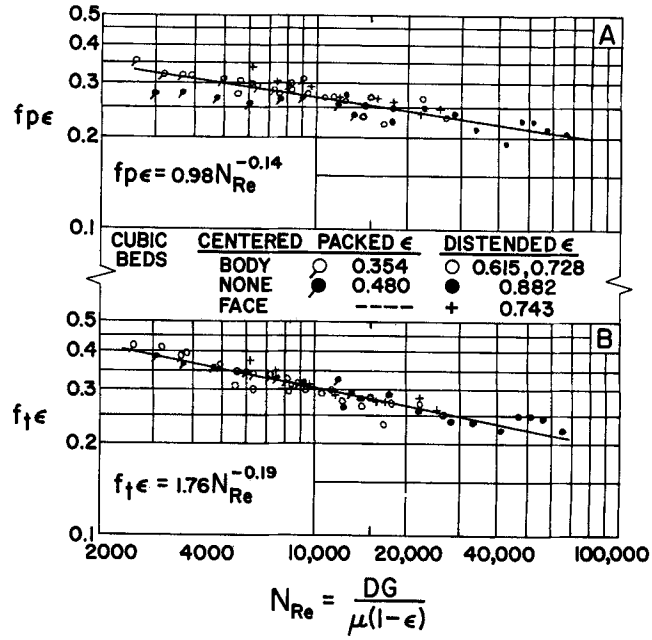

Fig. 1. Comparison of correlations with data. *A*. Form drag, Equation (8). *B*. Total drag, Equation (9).

Reynolds numbers. Within available precision, this analysis indicated that ($f_p\,\epsilon/2$) was a function only of N_{Re}. To the nearest 0.01 exponent, the resulting correlation is

$$f_p\,\epsilon/2 = 0.49\,N_{Re}^{-0.14} \qquad (8)$$

where $2{,}500 < N_{Re} < 65{,}000$

We then determined a new correlation of total drag and N_{Re}, using values of Wentz (*14*) as discussed in Appendix *B*. The resulting correlation, to the nearest 0.01 in exponent, is

$$f_t\,\epsilon/2 = 0.88\,N_{Re}^{-0.19} \qquad (9)$$

where $2{,}500 < N_{Re} < 65{,}000$

The fit of Equations (8) and (9) to the data, shown in Figure 1, is at least as good as that of the earlier correlation Equations (*6b*) and (*7*). The median deviation of the predicted drag numbers from the fifty-one data values is reduced from 7.2% [Equation (*7*)] to 3.9% [Equation (*8*)] for form drag and from 4.0% [Equation (*6b*)] to 3.0% [Equation (*9*)] for total drag. This improvement can also be observed by comparing Figure 1 with a similar plot of the earlier correlations (*16*). As noted in the original work, the form drag correlation has somewhat more scatter than the total drag correlation.

Figure 6 in Appendix *A* presents evidence indicating that the Reynolds number exponents of 0.14 and 0.19 in Equations (8) and (9) are noticeably different.

The exponential effect of N_{Re} on total drag was, as desired, determined independently of the form relationship. It is important to emphasize, however, that the effect of porosity was implicitly constrained by the choice of identical forms of the drag groups.

SHEAR DRAG

One estimate of shear drag was made by substituting the smooth correlations Equations (8) and (9) into the difference Equation (1). The result is

$$\frac{f_s\,\epsilon}{2} = \frac{0.88}{N_{Re}^{0.19}} - \frac{0.49}{N_{Re}^{0.14}} \qquad (10a)$$

This estimate is compared with form drag and total drag in Figure 2. Because the magnitude of the form drag

term is very nearly equal to that of the total drag in this region, the magnitude of shear drag calculated by difference is extremely sensitive to uncertainties. For example, the large range of expected shear drag deviations shown in Figure 2 is that predicted by using the rather conservative basis of median deviations ($\pm$ 3 and $\pm$ 4%). Because of the uncertainties, one would expect this study to illuminate only primary effects; it is expected that secondary parameters would be obscured by the inherent noise. Nevertheless, some significant conclusions can be drawn from Equation (10*a*).

Figure 2 indicates that the functional dependence of shear drag on N_{Re} is indeed quite different from that for form or total drag. For example, the log-log slope is larger for f_s than for f_p even at the lower values of N_{Re}. Furthermore, the slope tends to increase markedly at higher velocities.

Little quantitative information can be obtained in the higher N_{Re} region because uncertainties are so large, as shown in region *C* of Figure 2. The most reliable predictions are those in region *A*; here the slope is almost constant (0.42 to 0.52). As described in Appendix *B*, this lower speed portion of the shear drag curve (region *A*) can be represented within 1% by

$$\frac{f_s \epsilon}{2} = 1.29\, N_{Re}^{-0.46} \qquad (10b)$$

where $2{,}500 < N_{Re} < 7{,}000$. Equation (10*b*) was developed for comparison purposes. Because of its sensitivity to small changes in the constants of Equations (8) and (9), the exponent in Equation (10*b*) is not precise. Moreover, any description of region *B* would involve a larger exponent (0.52 to 0.72 here). Nevertheless, Equation (10*b*) gives quantitative evidence that the dependence of f_s on N_{Re} is quite different from that for f_p or f_t.

Another method of examining shear drag is to plot values for individual runs calculated from form and total drag data. A large amount of scatter would be expected, especially at higher Reynolds numbers on log-log coordinates (Figure 2). The semilog plot of Figure 3 shows a

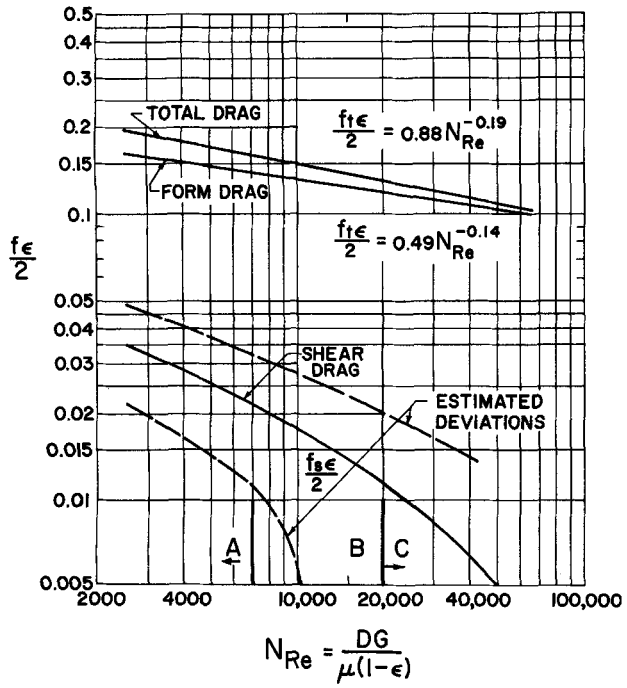

Fig. 2. Comparison of shear, form, and total drag correlations; Equations (10*a*), (8), and (9), respectively.

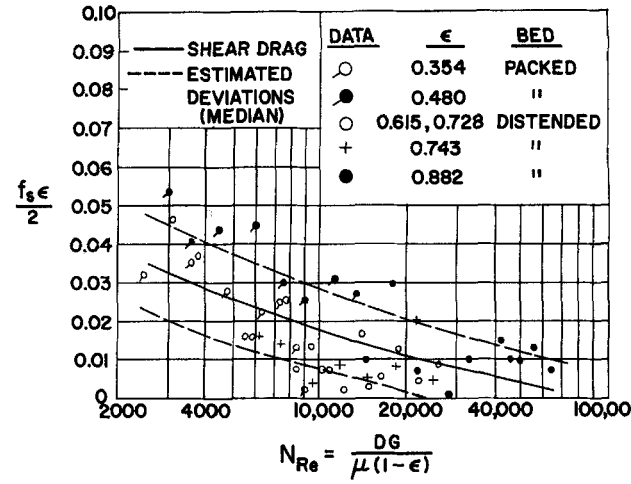

Fig. 3. Comparison of the shear drag correlation with data; Equation (10*a*) and conservative estimate of deviations.

comparison of shear drag difference data, such as those in Table 1, with the smoothed correlation Equation (10*a*). Most of the data fall within the deviation band shown. Many of the runs with high values can be explained by reference to Figure 1*A*, where the form drag values for the 0.480 porosity bed are seen to be considerably lower than most of the data, thereby resulting in much higher f_s values. By a similar examination of both plots in Figure 1, it can be seen that many values of the 0.615 and 0.728 porosity runs would be expected to be somewhat lower than the f_s correlation. When one considers that the deviation bands in Figure 3 are based on f_t and f_p deviations which were only 50% of the standard deviations, the agreement is unexpectedly good. This agreement was taken as approximate confirmation of Equations (10*a*) and (10*b*).

In view of the uncertainties in the shear drag data, the smoothed correlations are preferred for comparative study. In the 2,500 to 7,000 N_{Re} range, the effect of Reynolds number on shear drag was significantly larger (exponent of 0.46) than that on form drag (0.14) or on total drag (0.19).

Total drag is dependent on shear and form drag as shown in Equation (1). Therefore we expect that the effect of N_{Re} on f_t(0.19) is a weighted average of that on f_s and f_p (0.46 and 0.14). Moreover, the exponent on total drag is closer to that on form drag (as expected) because f_p is larger in magnitude than f_s in the region studied.

ESTIMATING DRAG RATIOS

One advantage of the independent determination of the influence of velocity on each of the three types of drags is that the relative size of any one type of drag may be estimated with respect to any other. The variations of these ratios, useful for understanding the mechanisms and for modeling, may then be estimated over a range of Reynolds numbers.

Moreover, if similar forms of correlation have been selected, the effect of various parameters on these ratios can be estimated easily, in many cases almost by inspection. We consider, for example, the lower velocity region of N_{Re} from 2,500 to 7,000. To determine the influence of velocity on the ratio of shear to total drag, we use Equations (10*b*) and (9) to predict that

$$\frac{f_s}{f_t} = 1.47\, N_{Re}^{-0.27} \qquad (11a)$$

where $2{,}500 < N_{Re} < 7{,}000$. Equation (11*a*) provides quantitative indication that the fraction of total drag due to shear decreases with increasing N_{Re} in this region. Some values taken from Equation (11*a*) indicate that the fraction is about 18% at N_{Re} of 2,500 and 13% at N_{Re} of 7,000. A estimate of the ratio at higher velocities can be obtained by dividing Equation (10*a*) by (9). Thus

$$\frac{f_s}{f_t} = 1 - 0.56\, N_{Re}^{0.05} \qquad (11b)$$

where $2{,}500 < N_{Re} < 65{,}000$. Equation (11*b*) indicates a ratio of 9% at $N_{Re} = 20{,}000$ and 2% at $N_{Re} = 65{,}000$. Comparison of these ratios with the 12% estimated by Wentz and Thodos (*16*) indicates that their value has the proper order of magnitude but is an approximate, average value which would be inappropriate for other velocities.

In the same manner one can estimate the ratio of shear to form drag. Where N_{Re} ranges are 2,500 to 7,000 and 2,500 to 65,000, respectively, we obtain

$$\frac{f_s}{f_p} = 2.6\, N_{Re}^{-0.32} \qquad (12a)$$

and

$$\frac{f_s}{f_p} = 1.80\, N_{Re}^{-0.05} - 1 \qquad (12b)$$

HEAT TRANSFER CORRELATIONS (LITERATURE)

The functional dependence of heat flux on velocity is useful for estimating whether any analogous behavior exists in beds of particles between heat transfer and shear drag. Correlations of heat flux have been determined in beds of spheres by a number of authors, but usually at a lower range of Reynolds number than that under study here.

McConnachie and Thodos (*10*) correlated heat flux data over a wide range of N_{Re} (70 to 7,000) and porosity by the following equation, using one packed ($\epsilon = 0.416$) and two distended ($\epsilon = 0.576$ and 0.778) beds at a Prandtl number of about 0.72:

$$N_{St}^{*}\, N_{Pr}^{2/3} = \frac{1.192}{N_{Re}^{0.41} - 1.52} \qquad (13)$$

The asterisk indicates that the heat flux was not corrected for end effects. Those authors reported that this correlation was in substantial agreement with the earlier work of Glaser and Thodos (*5*), who investigated a range of Prandtl numbers at Reynolds numbers up to 5,000 and with that of Gamson et al. (*4*), who studied packed beds up to Reynolds number of 3,000. The three-constant form of Equation (13) was chosen to describe small deviations from log-log linearity at Reynolds numbers below 400.

For comparative purposes, heat flux values from Equation (13) were fit to a simpler function over the Reynolds number range of 2,500 to 7,000. The result to the nearest 0.01 in exponent is

$$N_{St}^{*}\, N_{Pr}^{2/3} = 1.49\, N_{Re}^{-0.43} \qquad (14)$$

The maximum deviation of Equation (14) heat fluxes from those of Equation (13) is 0.5% in the N_{Re} range of 2,500 to 7,000 and 2% in the 300 to 7,000 range.

Gupta and Thodos (*16*) presented the following correlation of heat transfer data taken at the same Prandtl number using one packed ($\epsilon = 0.444$) and two distended ($\epsilon = 0.576$ and 0.778) beds

$$N_{St}\, N_{Pr}^{2/3}\, \epsilon = 2.06\, [N_{Re}\,(1-\epsilon)]^{-0.575} \qquad (15a)$$

where $400 < N_{Re} < 6{,}000$. Equation (15*a*) was also fitted to a two-constant form. The result, to the nearest 0.01 in exponent, is

$$N_{St}\, N_{Pr}^{2/3} = 6.4\, N_{Re}^{-0.58} \qquad (15b)$$

Equation (15*b*) agrees with Equation (15*a*) within a maximum deviation of 6% for all porosities and N_{Re} studied by Gupta and Thodos.

All the Stanton numbers used in this section are based on the integrated heat flux over the surface of a particle. We call this the *average heat flux.*

ANALOGOUS BEHAVIOR BETWEEN SHEAR DRAG AND HEAT TRANSFER

We restrict our discussion to cases where velocity profiles are not distorted appreciably by temperature profiles.

For flow through conduits or parallel to flat plates where form drag is negligibly small (zero form drag systems), the analogous behavior between shear drag and heat flux at the fluid-solid boundary has been studied extensively. Where two state properties of the fluid (molecular diffusivity of momentum and energy) happen to be equal ($N_{Pr} = 1$), this behavior may be expressed by the form known by Reynolds analogy:

$$N_{St} = f_s/2 \qquad (16a)$$

Many authors have attempted to correct for systems where the diffusion-rate properties are unequal. In the range of Prandtl number between 0.6 and 1,000, the simplest adjustment is an empirical one known as the *Chilton-Colburn anology.* This form, which implies the approximate assumption that the functional form of the correction is independent of Reynolds number, is

$$N_{St}\, N_{Pr}^{2/3} = f_s/2 \qquad (16b)$$

Henceforth, we refer to the product of N_{St} and $N_{Pr}^{2/3}$ as the adjusted Stanton number. (Since $N_{Pr} = 0.72$ for the data under study here, adjustment on N_{St} is quite small, merely 19%.)

For zero-form drag systems, the analogous behavior between heat flux and f_s has been well established by independent measurements of these two parameters. Equation (16*b*) has been found to be approximately valid in tests comparing magnitudes and influence of N_{Re} on average heat flux and average shear drag.

For systems where form drag is not negligible, testing for analogous behavior is more complex. Some evidence is given in Figure 4, which compares several of the equations of this paper and shows the differences between corrected and uncorrected heat flux data. The values of heat flux, f_t and f_p in Figure 4, provide quantitative evidence supporting the previously held view that the average heat flux is not analogous to either form or total drag for beds of spheres in this flow regime.

We now examine whether there is evidence of any kind of analogous behavior (in beds of spheres) between the adjusted N_{St} and f_s. Comparing the shear drag Equation (10*a*) with the heat correlation based on Gupta and Thodos, Equation (15*b*), we see from Figure 4 that the magnitudes of $f_s/2$ and adjusted N_{St} agree over the range in which both have been studied. The agreement in magnitude is, in fact, better than one would expect based on the uncertainties in the shear drag correlation.

We also see from Figure 4 that the functional dependencies of f_s and N_{St} on N_{Re} are very similar, certainly well within experimental precision. The shear drag Equation (10*a*) has local slopes varying from 0.42 to 0.57 in the region shown in Figure 4. Heat flux Equations (14) and (15*b*) have slopes of 0.43 and 0.58.

In addition to the 0.48 porosity used for the drag equations in Figure 4, there are three porosities used for

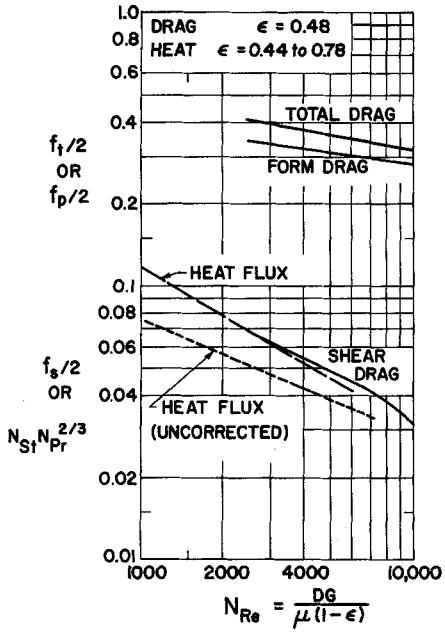

Fig. 4. Analogous behavior between shear drag and heat flux. A. Shear drag, Equation (10a). B. Heat flux, Equation (15b). C. Uncorrected heat flux, Equation (14).

drag tests which also lie within the heat flux correlation range: 0.615, 0.728, and 0.743. Predictions of shear drag for the 0.615 porosity bed are similar in magnitude to the uncorrected heat flux correlation shown in Figure 4. The predictions of shear drag for the higher porosities would lie somewhat below the uncorrected heat flux line in Figure 4. However, such predictions at 0.728 and 0.743 porosity are not directly comparable because only one run of each group of eight was taken at Reynolds numbers within the range for which the heat flux correlation has been tested; the other runs were taken at higher velocities (Table 3).

Other comments could be made about these effects, but they would be belaboring small differences due to porosity. Nowhere in this paper has there been a precise attempt to determine the specific effect of bed porosities on shear drag. In fact, the effect of porosity on form and total drag was constrained to be similar by the author in order to investigate the primary effect of N_{Re} (as emphasized in earlier sections). Therefore, no firm conclusion can be reached regarding the effect of porosity on the difference between total and form drag. Suffice it to say that the effect of porosity on shear drag is not completely understood, and further work in this area would be informative. It should also be noted that the lack of complete understanding of porosity does not indicate an absence of all kinds of analogous behavior.

Some scholars have felt little reason to suspect such analogous behavior in form drag systems. This feeling was partly based on theoretical arguments which noted the different nature of heat flux (vector) and shear stress (tensor) and noted that the equations of motion and energy may not seem analogous for this case. There is also the indication, based on experiments with single spheres in unbounded flow, that the local shear drag and local heat flux have different functional dependences on position.

However, none of these points removes the possibility of the kind of analogous behavior suggested in this work. More important to the question of the relationship between average fluxes (heat and momentum) in beds is the similar analogous behavior that has been reported by Tang et al. (*12*) for single spheres. Their studies involved a range of sphere Reynolds numbers from 200 to 2,000. There is also some evidence (*13*) that this analogous behavior between average flux values exists for spheres, within 10 to 20%, over a much wider range of sphere Reynolds number, 100 to 100,000.

We conclude that there is clear evidence of at least one kind of analogous behavior in beds of spheres in turbulent flow. The analogous behavior was found to exist between the average shear drag and the average heat flux and was based on experimental agreement of magnitude over a range of Reynolds numbers. It seems, however, to be a more limited analogy that the one found in zero-form drag systems. It is felt that further study is necessary.

Because the direct analogy between heat flux and mass flux is well known (*6*), the conclusions determined above and below should also apply to the similar relationship between average shear drag and average mass flux.

ESTIMATING DRAG COEFFICIENTS

The average value analogy described in the preceding section is a limited one, based pragmatically on experimental evidence. Since further work may limit some aspects of it, any use of it at this time must be made with certain reservations. It is in this respect and for illustration of possibilities that the following suggestions are given: prediction of shear drag from heat flux, prediction of form drag from pressure drop and heat flux, prediction of the ratio of shear to total drag, and prediction of the ratio of shear to form drag.

Where no other information is available, the shear drag might be estimated by using heat flux data and a zero-form drag analogy, such as

$$f_s{}^A/2 = N_{St}\,\phi \qquad (17)$$

where the superscript A denotes a term obtained by analogy. In general ϕ is a function of Prandtl number, Reynolds number, geometry, and other parameters. Several functions of both N_{Pr} and N_{Re} have been reported. Of course, if we take ϕ to be dependent only on state variables (N_{Pr}), we may use the Chilton-Colburn approximation of Equation (16*b*), and if we consider ϕ to be unity, we have Equation (16*a*). Because many such functions are available, no specific example of Equation (17) is given.

The second use involves prediction of form drag. Wentz and Thodos (*16*) have shown that determination of form drag in packed beds requires many tedious measurements. Where the average value analogy may be applied, the magnitude and functional dependence of form drag in packed bed flow can be more easily estimated by Equation (1) if pressure drop and heat flux data are available. For example, form drag may be estimated for the conditions of this study by subtracting the shear drag based on heat flux [Equations (15*b*) and (16*b*)] from the total drag, Equation (9). The result is

$$f_p{}^A\,\epsilon/2 = 0.88\,N_{Re}{}^{-0.19} - 6.4\,\epsilon\,N_{Re}{}^{-0.58} \qquad (18)$$

where $2{,}500 < N_{Re} < 6{,}000$ and $0.44 < \epsilon < 0.78$. Equation (18) agrees with form drag Equation (8) within a maximum deviation of 7%. It is interesting to note that the average deviation of Equation (18) from the form drag correlation Equation (8) was less than that of the original data, even though Equation (18) has anomalous, term-to-term variations in the dependence on porosity. This observation serves to emphasize that porosity effects are secondary in this work.

In the regions where shear drag is small compared with form drag, it is quite probable that the estimation of form drag by difference using Equation (1) may lead to more

accurate values than those determined by double integration of static pressure measurements. Moreover, measurement of both heat flux and pressure drop may be easier than the direct method. The disadvantage of bed end effects resulting from measurement of overall pressure drop and overall transfer rates may be minimized by using long beds.

Before discussing the other two predictions, we note parenthetically that total drag was estimated for comparative purposes by using the form drag Equation (8) and the shear drag based on heat flux, [Equations (15*b*) and (16*b*)]. The agreement was good; the average deviation of the predicted values from the data correlation [Equation (9)] was less than that of the original data.

The problem of estimating drag ratios has been discussed in an earlier section. We simply note alternate estimations based on the analogy for the case where $2{,}500 < N_{Re} < 6{,}000$ and $0.44 < \epsilon < 0.78$

$$f_s^A/f_t = 7.3\,\epsilon\,N_{Re}^{-0.39} \qquad (19a)$$

$$f_s^A/f_p = 13.1\,\epsilon\,N_{Re}^{-0.44} \qquad (19b)$$

SUMMARY

1. Based on the data of Wentz and Thodos, the influence of Reynolds number on form drag in beds of spheres was found to be about the −0.14 power and on total drag to be about the −0.19 power, both of which are somewhat different from that reported previously. Variables included a range of Reynolds numbers (2,500 to 65,000) and bed porosities (0.35 to 0.88).

2. The effect of Reynolds number on shear drag was found at lower velocities to be about the −0.46 power, which is significantly greater than that for form and total drag. The influence at higher Reynolds number was apparently −0.6 in exponent and greater.

3. The ratio of shear to total drag was found to vary with velocity, decreasing from about 18% at the lowest Reynolds number studied to below 5% at the highest value studied.

4. Experimental evidence in support of an apparently analogous behavior between average shear drag and average heat flux was presented. Reynolds numbers at which the average value analogy was tested were limited by existing data to the range from 2,500 to 6,000. Other limitations and related evidence were also discussed.

5. Methods for estimating the ratio of shear drag to form drag and for estimating drag coefficients were presented, based on the correlations of this work and the average value analogy.

NOTATION

A_s = surface area of all particles
A_x = open cross-sectional area of tube
C_p = heat capacity
D = particle diameter
F_n = form drag force
f_p = form drag, Equation (5), dimensionless
F_s = shear drag force
f_s = shear drag, Equation (3), dimensionless
F_t = total drag force
f_t = total drag, Equation (4), dimensionless
G = superficial mass velocity, ρU_s
h = heat transfer coefficient
I_n = normal stress integral, Equation (5*a*)
k = thermal conductivity
L = bed length
N_{Pr} = Prandtl number, $C_p\mu/k$, dimensionless
N_{Re} = Reynolds number, $DG/\mu(1-\epsilon)$, dimensionless
N_{St} = Stanton number, h/GC_p, dimensionless
P_n = normal pressure
P_S = static pressure
ΔP = pressure drop over bed length L
U_b = average velocity in the bed
U_s = superficial velocity (empty tube)

Greek Letters

α = offset angle (*16*)
β = angle of rotation (*16*)
ϵ = bed porosity, dimensionless
μ = viscosity
ϕ = function, Equation (17)
ρ = density
τ_s = average shear stress on the surface of the spheres

Superscripts

A predicted by using analogy
* = end effects uncorrected

LITERATURE CITED

1. Bird, R. B., W. E. Stewart, and E. N. Lightfoot, "Transport Phenomena," Chap. 6, Wiley, New York (1960).
2. Ergun, Sabri, *Chem. Eng. Progr.*, **48**, 89 (1952).
3. Cremer, H. W., and T. Davis, "Chemical Engineering Practice," Vol. 2, Academic Press, New York (1956).
4. Gamson, B. W., George Thodos, and O. A. Hougen, *Trans. Am. Inst. Chem. Engrs.*, **39**, 1 (1943).
5. Glaser, M. B., and George Thodos, *A.I.Ch.E. J.*, **4**, 63 (1958).
6. Gupta, A. S., and George Thodos, *ibid.*, **9**, 751 (1963).
7. Hastings, Cecil, "Approximations for Digital Computers," Princeton Univ. Press, N. J. (1955).
8. Martin, J. J., W. L. McCabe, and C. C. Monrad, *Chem. Eng. Progr.*, **47**, 91 (1951).
9. McCabe, W. L., and J. C. Smith, "Unit Operations of Chemical Engineering," pp. 94-97, McGraw-Hill, New York (1956).
10. McConnachie, J. T. L., and George Thodos, *A.I.Ch.E. J.*, **9**, 60 (1963).
11. Sherwood, T. K., and J. M. Petrie, *Ind. Eng. Chem.*, **24**, 736 (1932).
12. Tang, Y. S., J. M. Duncan, and H. E. Schweyer, *Natl. Advisory Comm. Aeronaut. Tech. Note 2867* (March, 1963).
13. Tallmadge, J. A., unpublished.
14. Wentz, C. A., Jr., Ph.D. dissertation, Northwestern Univ., Evanston, Ill. (1961).
15. ———, and George Thodos, *A.I.Ch.E. J.*, **9**, 81 (1963).
16. *Ibid.*, 358.

APPENDIX A: CORRELATION OF FORM DRAG DATA

This appendix describes the development of Equation (8) from form drag data of Tables 2 and 3.† It was assumed first that form drag was a function only of ϵ and N_{Re} and second that this function could be approximated by

$$f_p/2 = a\,N_{Re}^{\,b}\,\epsilon^c \qquad (A1)$$

where a, b, and c are constants. Because random errors were more constant expressed as percentages rather than absolute values (form drag only varied fivefold), linearization of Equation (A1) is suitable.

$$\log(f_p/2) = \log a + b\log N_{Re} + c\log\epsilon \qquad (A2)$$

To determine interpolation formulas, this linearization allowed the use of analytical expressions for polynomials developed from the least squares of the residuals. (The data were analyzed digitally, but for discussion some results are shown graphically.)

Determination of b and c was done in three steps: first porosity exponent, Reynolds exponent, and second porosity exponent.

The first porosity exponent was determined by using a two-step, cross-fit method similar to that used by Sherwood

† See footnote on page 600.

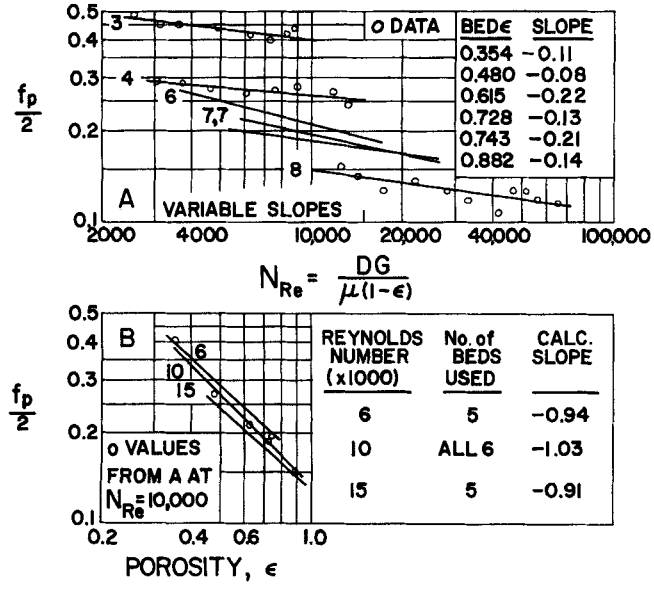

Fig. 5. Determination of the first porosity exponent. *A.* Interpolation at constant porosity. *B.* Slopes at constant Reynolds number.

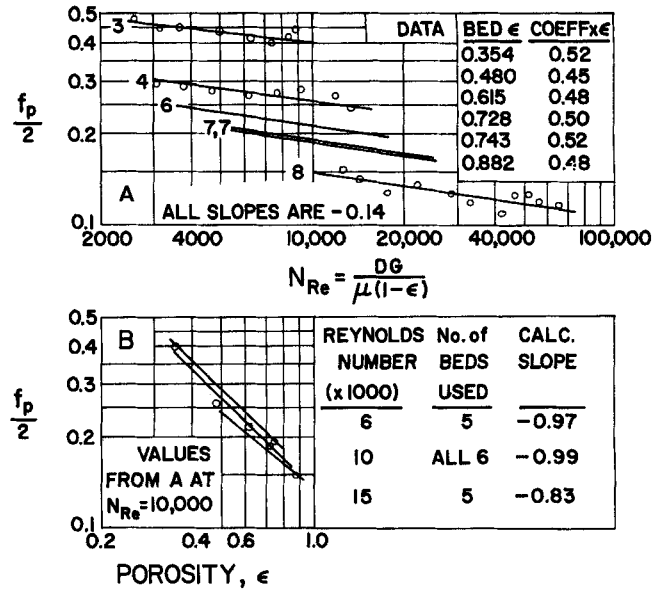

Fig. 7. Determination of the second porosity exponent. *A.* Constant porosity with 0.14 exponent. *B.* Slopes at constant Reynolds number.

and Petrie (*11*). Parameters a and b were estimated from constant ϵ formulas for each of six beds (Figure 5*A*). Then a and b were used to estimate smoothed values of form drag at three N_{Re}. Next exponent c was estimated from constant N_{Re} formulas at each of the three N_{Re}. As shown in Figure 5*B*, the average of the three porosity exponents was -0.96. Because the second figure was not considered significant, the first porosity exponent was taken to be -1.0. Thus Equation (*A*2) becomes

$$\log (f_p \epsilon/2) = \log a + b \log N_{Re} \qquad (A3)$$

The parameter $(f_p \epsilon/2)$ varied over a twofold range.

The Reynolds exponent was approximated by least squares of Equation (*A*3) to be -0.1415 and was rounded to -0.14 (Figure 6). Thus

$$[\log (f_p \epsilon/2) + 0.14 \log N_{Re}] = \log a \qquad (A4)$$

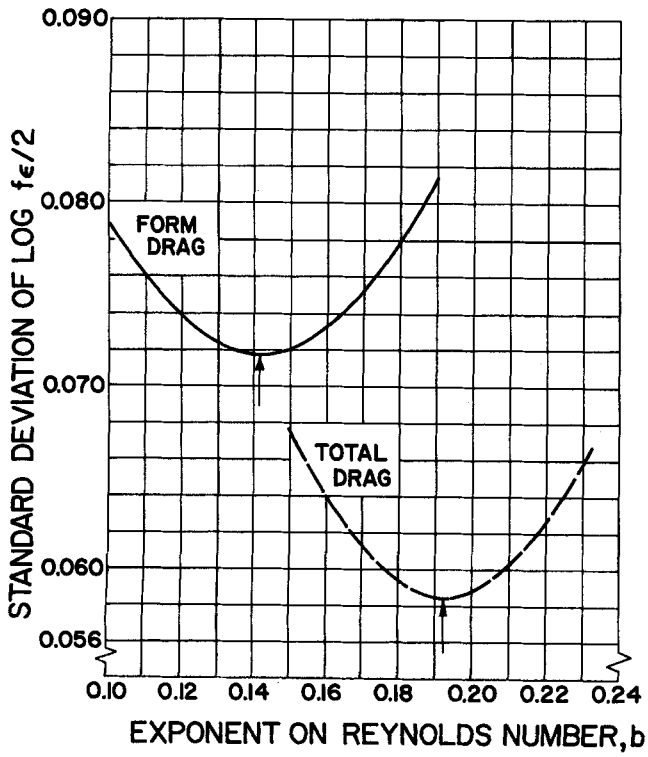

Fig. 6. Determination of the Reynolds number exponent.

by least squares of Equation (*A*4), $a = 0.4893$. Rounding, we obtain

$$f_p \epsilon/2 = 0.49\, N_{Re}^{-0.14} \qquad (A5)$$

The second porosity exponent was determined similarly to the first, except that b was constrained to be -0.14. Equation (*A*2) becomes

$$[\log (f_p/2) + 0.14 \log N_{Re}] = \log a + c \log \epsilon \qquad (A6)$$

This second porosity exponent was found to be -0.93 (Figure 7). Because -0.93 is nearly identical to -0.96, Equation (*A*5) was not adjusted further. Equation (*A*5) describes all fifty-one data values with deviations of 4.0% (median), 5.5% (average), 7.4% (standard), and 16.1% (maximum). Ninety percent of the runs were within 13.5% of Equation (*A*5), and the standard deviation of $(f_p \epsilon/2)$ was 0.0097. Equation (*A*5) is compared with data of three beds in Figure 7*A*.

APPENDIX *B*: OTHER CORRELATIONS

This appendix describes both how Equation (9) was developed from the fifty-one total drag values and how one equation was fit with another. For total drag, we first selected the porosity-adjusted group $(f_t \epsilon/2)$ for correlation. This group was chosen partly because of similarity to form drag [Equation (8)] but primarily because of its previous correlation success (*1, 2, 9, 15*). Second, the functional dependence was assumed to be

$$\log (f_t \epsilon/2) = \log a + b \log N_{Re} \qquad (B1)$$

When one fits Equation (*B*1) as with Equation (*A*3), b is approximated as -0.1920 and rounded to -0.19 (Figure 6). Similar to Equation (*A*4), the constant was found to be 0.878 and then rounded. The desired result, Equation (9), describes the fifty-one values with deviations of 3.0% (median), 4.3% (average), 5.9% (standard), and 19.9% (maximum). Ninety percent of the runs were within 9.7%; the standard deviation of $(f_t \epsilon/2)$ was 0.0086.

Values from smooth correlations were fit to the Equation (*B*2) form with least maximum deviation, as recommended by Hastings (7):

$$f \epsilon/2 = a\, N_{Re}^{b} \qquad (B2)$$

Two one-dimensional searches were made: the first to select b with least range of percent deviation and then second to select the coefficient (a) with least maximum deviation. All equations of the Equation (*B*2) form were fit in this way.

Manuscript received July 20, 1966; revision received October 18, 1966; paper accepted October 18, 1966.